FAP-targeted radioligand therapy with ^{68}Ga/^{177}Lu-DOTA-2P(FAPI)$_2$ enhance immunogenicity and synergize with PD-L1 inhibitors for improved antitumor efficacy

Jianhao Chen,[1,2] Yangfan Zhou,[1,3] Yizhen Pang,[1,3] Kaili Fu,[4] Qicong Luo ,[5] Long Sun,[1] Hua Wu,[1] Qin Lin,[3] Guoqiang Su,[2] Xiaoyuan Chen ,[6,7,8,9] Liang Zhao,[1] Haojun Chen [1]

For numbered affiliations see end of article.

Correspondence to
Dr Haojun Chen;
leochen0821@foxmail.com

Dr Liang Zhao;
wzhaoliang01@163.com

Xiaoyuan Chen;
chen.shawn@nus.edu.sg

Dr Guoqiang Su;
suguoqiang66@163.com

ABSTRACT

Background Fibroblast activation protein (FAP)-targeted radioligand therapy, with immunomodulatory effects, has shown efficacy in both preclinical and clinical studies. We recently reported on a novel dimeric FAP-targeting radiopharmaceutical, ^{68}Ga/^{177}Lu-DOTA-2P(FAPI)$_2$, which demonstrated increased tumor uptake and prolonged retention in various cancers. However, further exploration is required to understand the therapeutic efficacy and underlying mechanisms of combining ^{68}Ga/^{177}Lu-DOTA-2P(FAPI)$_2$ radioligand therapy with PD-1/PD-L1 immunotherapy.

Methods Regarding the change in PD-L1 expression and DNA double-strand breaks induced by radiopharmaceuticals, CT26-FAP tumor cells were incubated with ^{68}Ga and ^{177}Lu labeled DOTA-2P(FAPI)$_2$, respectively. Monotherapy with ^{68}Ga-DOTA-2P(FAPI)$_2$, ^{177}Lu-DOTA-2P(FAPI)$_2$, and PD-L1 immunotherapy as well as combination therapy (^{68}Ga/^{177}Lu-DOTA-2P(FAPI)$_2$ and PD-L1 immunotherapy) were tested and evaluated to evaluate in vivo antitumor efficacy. Furthermore, immunohistochemical staining and single-cell RNA sequencing were used to analyze changes in the tumor microenvironment (TME) and elucidate the underlying mechanisms of action of this combination therapy.

Results Our findings indicated that FAP-targeting radiopharmaceuticals can induce DNA double-strand breaks and upregulate PD-L1 expression, with ^{177}Lu-DOTA-2P(FAPI)$_2$ proving to be more effective than ^{68}Ga-DOTA-2P(FAPI)$_2$. Both ^{68}Ga-DOTA-2P(FAPI)$_2$ and ^{177}Lu-DOTA-2P(FAPI)$_2$ radiopharmaceuticals significantly improved therapeutic outcomes when combined with anti-PD-L1 monoclonal antibody (αPD-L1 mAb). Notably, the combination of ^{177}Lu-DOTA-2P(FAPI)$_2$ with αPD-L1 mAb immunotherapy eliminated tumors in mouse models. Mice treated with this regimen not only exhibited exceptional responses to the initial immune checkpoint inhibitor therapy but also showed 100% tumor rejection on subsequent tumor cell re-inoculation. Further mechanistic studies have shown that ^{177}Lu-DOTA-2P(FAPI)$_2$ combined with αPD-L1 mAb can reprogram the TME, enhancing antitumor intercellular communication, which activates

WHAT IS ALREADY KNOWN ON THIS TOPIC

⇒ Immune checkpoint blockade immunotherapy alone often yields low response rates, benefiting only a minority of patients. Fibroblast activation protein (FAP) is a broad target in the tumor microenvironment (TME), and previous research has demonstrated that FAP-targeting radioligand therapy is effective in both preclinical and clinical studies, with immunomodulatory effects. We have designed and synthesized a novel dimeric FAP-targeting radiopharmaceutical, ^{68}Ga/^{177}Lu-DOTA-2P(FAPI)$_2$, which demonstrated increased tumor uptake and prolonged retention in various cancers.

WHAT THIS STUDY ADDS

⇒ Combining ^{177}Lu-DOTA-2P(FAPI)$_2$ radioligand therapy with αPD-L1 mAb immunotherapy significantly enhances TME modulation, leading to increased infiltration of CD8+ T-cells and mature antitumor neutrophils, and the combination therapy reprograms the TME, substantially improving the rate of complete remission and prolonging overall survival.

HOW THIS STUDY MIGHT AFFECT RESEARCH, PRACTICE OR POLICY

⇒ ^{177}Lu-DOTA-2P(FAPI)$_2$ radioligand therapy, combined with PD-L1 immunotherapy, can potentially increase the efficacy and sensitivity to immunotherapy, enables a translatable approach to promoting response to PD-1/PD-L1 inhibitors. This underscores the necessity for pilot clinical trials to assess the effectiveness of this combination therapy, which could potentially impact future treatment guidelines and improve outcomes for patients with difficult-to-treat tumors.

antitumor-related intercellular contacts such as FasL-Fas interactions between T cells and NK cells with tumor cells and increasing the proportion of infiltrating CD8+ T-cells while reducing regulatory T cells and inhibiting tumor progression. Our research also demonstrates that mature

neutrophils play a role in enhancing the efficacy of the combined therapy, as shown in neutrophil-blocking experiments.

Conclusions Our study robustly advocates for use of FAP-targeting radiopharmaceuticals, particularly ^{177}Lu-DOTA-2P(FAPI)$_2$, alongside immunotherapy in treating FAP-positive tumors. This combination therapy transforms the TME and enables a translatable approach to increasing the sensitivity to PD-1/PD-L1 immunotherapy, leading to improved complete remission rates and extended overall survival.

BACKGROUND

The progress in immunotherapy has fundamentally altered cancer treatments. Immune checkpoint inhibitors (ICIs), such as PD-1/PD-L1, have improved the survival rates of certain patients with late-stage cancer. However, despite some patients experiencing long-term or complete tumor regression with ICIs treatment, clinical trials have shown that the overall response rate of patients with tumors receiving ICIs monotherapy is approximately 20%–30%.[1] Previous studies have demonstrated that patients with microsatellite stable (MSS) colorectal cancer (CRC) are less responsive to immunotherapies such as PD-1/PD-L1 blockade, while patients with microsatellite instability-high (MSI-H) CRC, due to their higher mutational burden and greater immune activation, are more sensitive to such therapies.[2 3] The response rate is particularly low for MSS-CRC, characterized by their typically low mutational burden, and immune activation.[2 3] Therefore, the development of safe and efficient combination therapy strategies is essential to convert the tumor microenvironment (TME) of MSS-CRC for increasing the efficacy and sensitivity to PD-1/PD-L1 immunotherapy.

External beam radiation therapy (EBRT) has always been a focus of attention in oncology. Preclinical studies have shown that EBRT can induce direct tumor cell death via ionizing radiation and immunogenic cell death, leading to an in situ tumor vaccine effect. EBRT can induce local inflammation while simultaneously upregulating the expression of PD-L1 in the TME. Multiple studies have indicated that combining EBRT with ICIs therapy can boost systemic antitumor immune responses.[4 5] However, the application of EBRT in patients with extensive systemic metastatic tumors or tumors adjacent to vital organs poses significant challenges.

Targeted radionuclide therapy (TRT) is an option for treating patients with widespread metastatic tumors. Compared with EBRT, TRT can selectively deliver radiation to cancer cells while minimizing exposure to healthy tissues. Therapeutic and diagnostic radionuclides are pivotal in oncological research; however, they affect the TME in distinct ways. Therapeutic radionuclides, including ^{177}Lu, ^{90}Y, and [211]At, are highly valued for delivering continuous radiation that can directly kill or suppress tumor cells. These radionuclides exhibit sustained therapeutic effects. Our research team previously used ^{177}Lu-EB-RGD to target integrin $\alpha_v\beta_3$ in MC38 colorectal tumor-bearing mice, which increased immune cell infiltration in the TME, up-regulating PD-L1 and enhancing the antitumor effect of MC38 tumors when combined with αPD-L1 mAb.[6] In contrast, nuclear imaging radionuclides, including ^{18}F, ^{68}Ga, and ^{99m}Tc, are primarily used for diagnostic purposes in clinical settings. Theoretically, diagnostic radionuclides can damage DNA and induce apoptosis or necrosis in tumor cells by emitting positrons,[7] especially at higher doses, through released positrons to produce some cytotoxic effects.[8] Previous preclinical studies found that the imaging radionuclide ^{18}F-FDG induces apoptosis necrosis of tumor cells in tumor-bearing mice, with modest therapeutic responses observed, making it a potential candidate for treating tumors.[8 9] The energy of positrons (β+) emitted by ^{18}F is approximately 0.633 MeV, close to the energy of electrons (β−) emitted by ^{131}I at 0.606 MeV.[10] In contrast, β+ from ^{68}Ga is about 1.9 MeV, approximately three times stronger than that of [18]F. Further preclinical study demonstrated that in MC38 (MSI-H) and CT26 (MSS-CRC) tumor-bearing mice,[11] ^{18}F-FDG increased T-cell infiltration, upregulated tumor cell PD-L1 expression, remodeled TME, and improved the efficacy of combination therapy with αPD-L1 mAb.[12] These studies suggest that diagnostic radionuclides are potential partners that can unlock the full therapeutic potential of ICIs. However, no relevant studies have compared the effects of therapeutic and diagnostic radionuclides on the modulation of the tumor immune microenvironment and their antitumor efficacy.

Fibroblast activation protein (FAP) is a key target in radiopharmaceutical development.[13] In many epithelial cancers, FAP is predominantly expressed in cancer-associated fibroblasts (CAFs) within the TME. Its expression is notable in tumor cells across sarcomas and mesotheliomas and sporadically in epithelial tumors, including head and neck squamous cell carcinoma and esophageal cancer.[13] FAP-targeting radiopharmaceuticals, such as ^{177}Lu or ^{90}Y labeled FAP-inhibitor (FAPI) molecules (FAPI-04 and FAPI-46), have been evaluated in patients with various advanced tumors, showing favorable safety profiles and potential for treating refractory cancers. However, the therapeutic effectiveness of these initial studies is still limited, primarily because of the relatively short tumor retention of current FAPI molecules. We have recently developed a novel FAP-targeting dimeric molecule, DOTA-2P(FAPI)$_2$, which demonstrated significant improvements in FAP-targeting efficacy, resulting in increased tumor uptake and prolonged retention in preclinical and clinical studies.[14] In subsequent therapy experiments, TRT with ^{177}Lu-DOTA-2P(FAPI)$_2$ demonstrated superior antitumor effects compared with conventional ^{177}Lu-FAPI-46.[15]

In this study, we explored the immunomodulatory potential of ^{68}Ga-DOTA-2P(FAPI)$_2$ and ^{177}Lu-DOTA-2P(FAPI)$_2$ as immunomodulators in a mouse model of MSS-CRC. This study aimed to determine whether these FAP-targeted radiopharmaceuticals can enhance the efficacy of anti-PD-1/PD-L1 immunotherapy and to elucidate the underlying mechanisms. We hypothesized

that such an approach might improve treatment outcomes by transforming the immunosuppressive TME into an environment more conducive to effective immunotherapy.

MATERIALS AND METHODS
^{68}Ga-DOTA-2P(FAPI)$_2$ and ^{177}Lu-DOTA-2P(FAPI)$_2$ radiolabeling

Radiolabeling of FAPI variants followed the protocol reported in our previous studies.[14 15] Regarding ^{68}Ga labeling, approximately 25 nmol of FAPI-46 and DOTA-2P(FAPI)$_2$ was dissolved in 1 mL of NaAc (0.25 M aqueous solution), and 4 mL of ^{68}GaCl$_3$ solution (1.1 GBq, dissolved in 0.05 M HCl) was added. The mixture was allowed to react at 100°C for 15 min. Concerning ^{177}Lu labeling, the precursors were dissolved in 1 mL of NH$_4$OAc (0.25 M aqueous solution) and added to 4 mL of ^{177}LuCl$_3$ solution (0.7 GBq, 0.05 mol/L HCl solution). The mixture was incubated at 95°C for 30 min. The products of ^{68}Ga labeling or ^{177}Lu labeling were purified using a C18 column (WAT020515, Waters Corporation), and the radioactive labeling efficiency and radiochemical purity were tested using thin-layer chromatography and high-performance liquid chromatography.[15]

In vitro evaluation

For cellular uptake and inhibition experiments, CT26-FAP and CT26 cells were seeded in 24-well plates (2×10^5 cells/well) overnight. Cells were incubated with 37 kBq of ^{68}Ga-DOTA-2P(FAPI)$_2$ at 37°C for 10, 30, or 60 min in a serum-free medium. In the inhibition group, unlabeled FAPI-46 (10 µg/well) was added as an inhibitor. At each time, the medium was removed, and the cells were washed twice with cold phosphate-buffered saline (PBS) (pH 7.4) and then lysed with 0.5 mL of NaOH (0.1 M). Cell lysates were collected, and the radioactivity was measured using a γ-counter. Each experiment was repeated thrice. Regarding the regulation of PD-L1 expression in tumor cells by radiopharmaceuticals, CT26-FAP cells incubated with 3.7 MBq/mL ^{68}Ga-DOTA-2P(FAPI)$_2$ and ^{177}Lu-DOTA-2P(FAPI)$_2$ respectively, for 4 hours and 24 hours and then replaced with serum-free medium. The experimental details of cell culture, western blotting, flow cytometry, and immunofluorescence are available in online supplemental material.

Establishment of CT26-FAP tumor-bearing mice

BALB/c mice aged 6–8 weeks were housed at the Xiamen University Laboratory Animal Center under SPF conditions. CT26-FAP cell suspension (approximately 2×10^6 cells resuspended in 100 µL PBS) was injected subcutaneously into the right thigh root of BALB/c mice. Radioactive nuclide treatment experiments were performed when the tumor volume reached 50 mm^3. Small animal PET and SPECT imaging studies were conducted when the tumor volume reached around 300 mm^3.

Small-animal PET/SPECT imaging and biodistribution study

Approximately 7.4 MBq of ^{68}Ga-FAPI-46 and ^{68}Ga-DOTA-2P(FAPI)$_2$ was injected intravenously into CT26-FAP tumor-bearing mice (n=3/group) for PET imaging. The time points for data collection were 1, 2, and 4 hours post-injection. Regions of interest for the tumor, liver, heart, kidneys, and muscles were quantified for radioactive signals on the PET images. Approximately 18.5 MBq ^{177}Lu-DOTA-2P(FAPI)$_2$ was injected intravenously into CT26-FAP tumor-bearing mice (n=3/group) for SPECT imaging. Whole-body SPECT images were acquired at 4, 24, 48, 72, and 96 hours post-injection. The acquisition parameters included a 20% window width for ^{177}Lu, a matrix size of 256×256, and medium zoom with 48 frames at energy peak values of 112.9 and 208.4 keV. The mice were anesthetized with 1.5% isoflurane during imaging to maintain spontaneous respiration.

A biodistribution study was conducted using CT26-FAP tumor-bearing mice. Mice were injected with 0.74 MBq of ^{177}Lu-DOTA-2P(FAPI)$_2$ (n=3/group). Major organs and tumors were collected and weighed at 4, 24, 48, and 72 hours post-injection. Radioactivity was detected using a γ-counter, and biodistribution results were calculated as a percentage of injected dose per gram (%ID/g).

In vivo antitumor efficacy and histopathological analysis

When the tumor volume reached 50 mm^3, the CT26-FAP tumor-bearing mice were randomly divided into six treatment groups (n=6/group): group A: treated with saline as control. Group B: received αPD-L1 mAb at a dose of 10 mg/kg on days 0, 3, and 6. Group C: injected with 29.6 MBq of ^{68}Ga-DOTA-2P(FAPI)$_2$ on days 0, 2, 4, and 6. Group D: received combined therapy of 29.6 MBq of ^{68}Ga-DOTA-2P(FAPI)$_2$ and 10 mg/kg of αPD-L1 mAb. Group E: treated with 18.5 MBq ^{177}Lu-DOTA-2P(FAPI)$_2$ on day 0. Group F: received combined therapy, consisting of 18.5 MBq of ^{177}Lu-DOTA-2P(FAPI)$_2$ and 10 mg/kg of αPD-L1 mAb (BE0101, BioXCell, USA). Body weight and tumor volume were monitored every 2 days post-treatment. The tumor size (mm^3) was calculated using the formula length×width×width/2. The mice were euthanized once weight loss reached 20% or tumor volume exceeded 1500 mm^3.

To assess the histopathological response of tumor tissues after TRT, we collected tumor samples from each group of CT26-FAP tumor-bearing mice on day 7 post-treatment. Immunohistochemical (IHC) staining was performed on tumor tissue samples for CD31 mAb (ab9498, Abcam), Ki-67 mAb (ab15580, Abcam), CD8+ T cell mAb (ab217344, Abcam), and GZMB mAb (ab4059, Abcam), according to previous protocols.[6] To evaluate the effect of TRT on normal organs, major organs, including the heart, liver, spleen, lungs, kidneys, and muscles, were collected from each group and subjected to H&E staining.

Regarding the neutrophil blockade experiment, when the tumor volume reached 50 mm^3, the CT26-FAP tumor-bearing mice were randomly divided into four treatment groups (n=6/group): group A: treated with saline

as control. Group B: received αLy6G mAb (BE0075-1, BioXCell, USA) for neutrophil depletion at a dose of 10 mg/kg, three times a week for 3 weeks. Group C: received combined therapy, consisting of 18.5 MBq of ^{177}Lu-DOTA-2P(FAPI)$_2$ and 10 mg/kg of αPD-L1 mAb. Group D: received 18.5 MBq of ^{177}Lu-DOTA-2P(FAPI)$_2$, 10 mg/kg of αPD-L1 mAb, and αLy6G mAb. Regarding the CD8+ T cell blockade experiment, when the tumor volume reached 50 mm^3, the CT26-FAP tumor-bearing mice were randomly divided into two treatment groups (n=6/group): group A: received 18.5 MBq of ^{177}Lu-DOTA-2P(FAPI)$_2$. Group B: received αCD8 mAb (BP0117, BioX-Cell, USA) for CD8+ T cell depletion at a dose of 10 mg/kg, three times a week for 2 weeks and received 18.5 MBq of ^{177}Lu-DOTA-2P(FAPI)$_2$.

Isolating single cells from mouse tumor tissues and single-cell RNA sequencing

Single-cell suspensions were loaded on 10 K Genomics-Perseus according to the manufacturer's protocol based on the 10 K GEMCode proprietary technology (10K Genomics, Shanghai, China). According to the manufacturer's protocol, single-cell RNA sequencing (scRNA-seq) libraries were prepared using the 10 K Genomics-Perseus Single Cell 3 Reagent Kit. The initial step involved creating an emulsion in which individual cells were isolated into droplets and gel beads coated with unique primers bearing 10 K cell barcodes, unique molecular identifiers, and poly(dT) sequences. Reverse transcription reactions were performed to generate barcoded full-length cDNA, followed by disruption of the emulsions using a recovery agent and cDNA cleanup. Bulk cDNA was amplified and cleaned up. Sequencing libraries were constructed using the reagents from the 10 K Genomics-Perseus Single Cell 3′ Reagent Kit, following these steps: (1) fragmentation, end repair, and a-tailing; (2) size selection with SPRI select; (3) adaptor ligation; (4) post ligation cleanup with SPRI select; (5) sample index PCR and cleanup with SPRI select beads. Indexed libraries were pooled according to the number of cells and sequenced on a NovaSeq 6000 (Illumina) using 150 bp paired ends.

Statistical analysis

All statistical analyses were performed using SPSS (V.22.0; IBM, Armonk, NY, USA). One-way analysis of variance and Student's t-tests were used to compare the means. Data are presented as the mean±SD. Statistical significance was defined as *p<0.05; **p<0.01; ***p<0.001; and ****p<0.0001; ns=not significant.

RESULTS

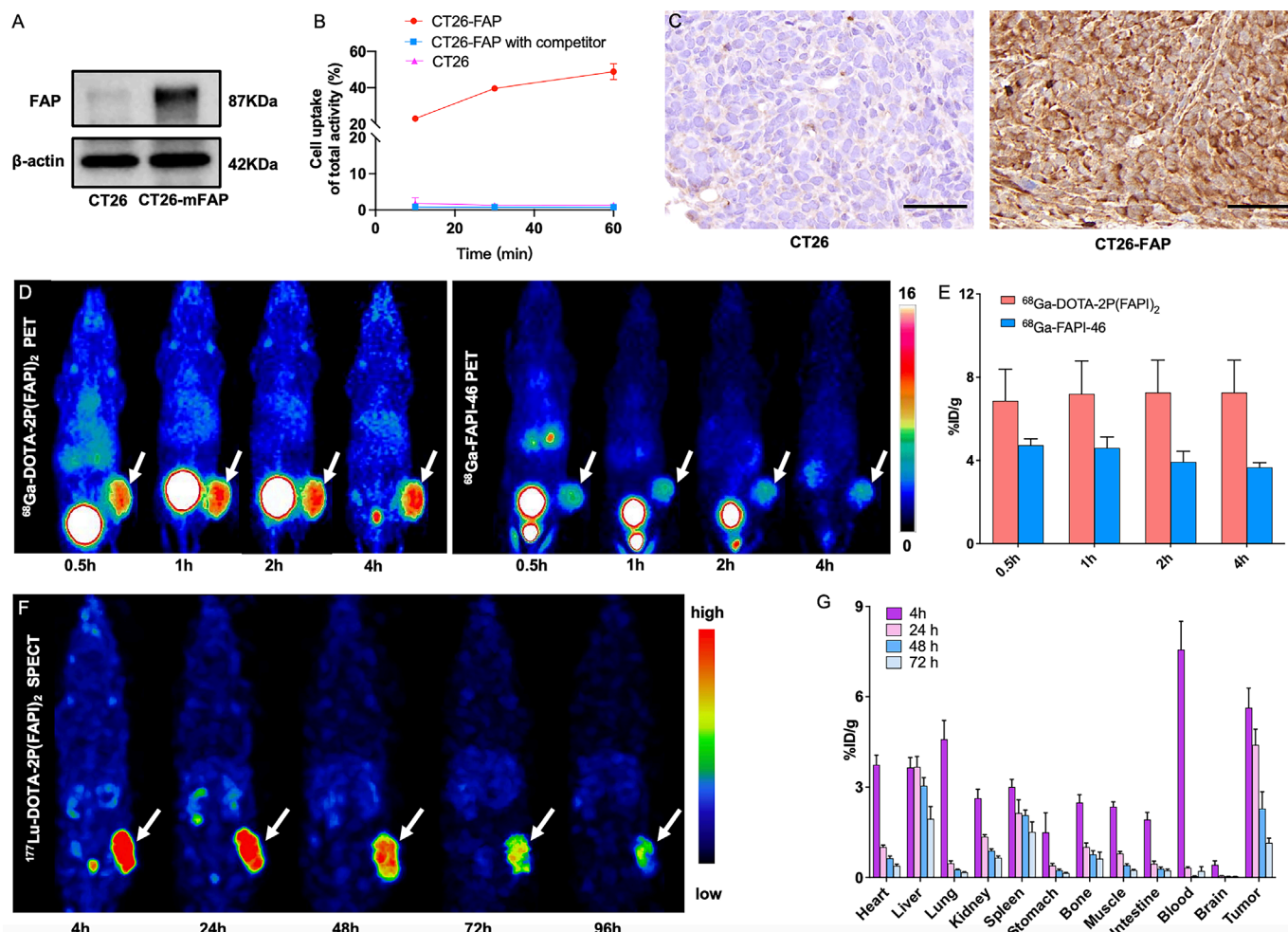### In vitro and in vivo evaluation of ^{68}Ga/^{177}Lu-DOTA-2P(FAPI)$_2$

Following purification, the radiochemical purity of all products exceeded 95%. The average specific activities of ^{68}Ga-DOTA-2P(FAPI)$_2$ and ^{68}Ga-FAPI-46 were 12–16 GBq/μmol, and the specific activity of ^{177}Lu-DOTA-2P(FAPI)$_2$ was 22–24 GBq/μmol. Western blot analysis showed

higher FAP expression in the CT26-FAP cell line, whereas it was negative in CT26 cells (figure 1A). Cellular uptake and blocking experiments revealed a gradual increase in ^{68}Ga-DOTA-2P(FAPI)$_2$ uptake by CT26-FAP cells over 10–60 min (figure 1B). In contrast, the CT26-FAP blocking and CT26 control groups exhibited significantly lower uptake values, indicating strong target specificity and affinity for DOTA-2P(FAPI)$_2$ in CT26-FAP cells. IHC analysis revealed high FAP expression in CT26-FAP tumor tissues, whereas FAP was largely absent in CT26 tumor tissues (figure 1C).

PET and SPECT imaging were used to assess and quantify the uptake pattern of ^{68}Ga-DOTA-2P(FAPI)$_2$, ^{68}Ga-FAPI-46, and ^{177}Lu-DOTA-2P(FAPI)$_2$ in CT26-FAP tumor-bearing mice. Tumor uptake of ^{68}Ga-DOTA-2P(FAPI)$_2$ and ^{68}Ga-FAPI-46 was rapid and intense at 0.5 hours post-injection. At 2–4 hours post-injection, the tumor uptake of ^{68}Ga-FAPI-46 gradually decreased, whereas that of ^{68}Ga-DOTA-2P(FAPI)$_2$ remained stable up to 4 hours post-injection (figure 1D). Quantitative analysis data for the tumor and normal organs from PET imaging are presented in figure 1E. SPECT imaging with ^{177}Lu-DOTA-2P(FAPI)$_2$ was conducted to investigate the in vivo biological behavior of DOTA-2P(FAPI)$_2$ at various time points in CT26-FAP tumor-bearing mice. Representative whole-body maximum intensity projections from tumor-bearing mice are shown in figure 1F. The biodistribution data correlated with the SPECT results, showing the highest uptake of ^{177}Lu-DOTA-2P(FAPI)$_2$ 24 hours post-injection, followed by a gradual decrease in the uptake from 24 hours to 72 hours post-injection (figure 1G).

Upregulated tumor PD-L1 expression after ^{68}Ga/^{177}Lu-DOTA-2P(FAPI)$_2$ stimulation both in vitro and in vivo

Flow cytometry analysis revealed a low percentage of PD-L1-positive cells in untreated tumor samples, consistent with findings from previous studies.[12 16] The negative control, using an isotype control for the PD-L1 antibody with CT26-FAP cells, is presented in online supplemental figure S1. Notably, the proportion of PD-L1-positive cells increased significantly following 24 hours stimulation with ^{68}Ga-DOTA-2P(FAPI)$_2$ and both 4 hours and 24 hours stimulation with ^{177}Lu-DOTA-2P(FAPI)$_2$. The proportion of PD-L1 positive cells was significantly lower in the untreated control tumors after only 4 hours of stimulation with ^{68}Ga-DOTA-2P(FAPI)$_2$ (figure 2A,B). Immunofluorescence staining of PD-L1 in CT26-FAP tumor cells after ^{68}Ga/^{177}Lu-DOTA-2P(FAPI)$_2$ stimulation yielded consistent results (figure 2C,D). IHC examination showed enhanced PD-L1 expression in tumor tissues after administering ^{68}Ga/^{177}Lu-DOTA-2P(FAPI)$_2$ (figure 2E). Immunofluorescence staining of γ-H2AX in CT26-FAP tumor cells post-stimulation with ^{68}Ga/^{177}Lu-DOTA-2P(FAPI)$_2$ revealed DNA double-strand breaks, with ^{177}Lu-DOTA-2P(FAPI)$_2$ showing the most significant effects (figure 2F,G) compared with the control group.

Figure 1 In vitro and in vivo evaluation of ^{68}Ga/^{177}Lu-labeled DOTA-2P(FAPI)$_2$. (A) Fibroblast activation protein (FAP) expression in CT26-FAP cells was determined using western blotting. (B) Cell uptake and blocking assays of ^{68}Ga-DOTA-2P(FAPI)$_2$ on CT26-FAP and CT26 tumor cells. (C) Immunohistochemical staining of FAP in tumor tissues. Scale bar: 50 µm. (D) Representative static PET images of ^{68}Ga-DOTA-2P(FAPI)$_2$ and ^{68}Ga-FAPI-46 in CT26-FAP tumor-bearing mice. (E) PET quantification data for ^{68}Ga-DOTA-2P(FAPI)$_2$ and ^{68}Ga-FAPI-46 in CT26-FAP tumor-bearing mice. (F) SPECT MIP images of ^{177}Lu-DOTA-2P(FAPI)$_2$ from 4 to 96 hours after injection in CT26-FAP tumor-bearing mice. (G) Biodistribution of ^{177}Lu-DOTA-2P(FAPI)$_2$ from 4 to 72 hours after injection in CT26-FAP tumor-bearing mice (n=3/group).

Combination of ^{177}Lu-DOTA-2P(FAPI)$_2$ with αPD-L1 mAb results in the most significant tumor growth delay and overall survival improvement

We subsequently conducted a further study on the immunomodulatory effects of ^{68}Ga/^{177}Lu-DOTA-2P(FAPI)$_2$ in combination with αPD-L1 mAb on delaying the growth of CT26-FAP tumor-bearing mice (figure 3A). In the vehicle group, tumor-bearing mice exhibited rapid tumor growth, leading to 100% tumor-related mortality by day 24 post-treatment. Despite the slower tumor growth rates in the αPD-L1 mAb and ^{68}Ga-DOTA-2P(FAPI)$_2$, all mice succumbed on day 30. In the treatment group of ^{177}Lu-DOTA-2P(FAPI)$_2$ and ^{68}Ga-DOTA-2P(FAPI)$_2$ combined with αPD-L1 mAb, two out of six mice succumbed on day 30 (figure 3B). The αPD-L1 mAb and ^{177}Lu-DOTA-2P(FAPI)$_2$ combination therapy group demonstrated the best antitumor effect, with all mice achieving complete remission (CR) by day 16 post-treatment (figure 3B–D). To evaluate the persistence of immune memory, on the 91st

day of treatment, we simultaneously injected CT26-FAP tumor cells (approximately 2×10^6 cells resuspended in 100 µL PBS) into the left posterior side of the healed mice for reattack and did not observe any tumor recurrence for at least 2 months. This suggests that radioligand therapy when combined with blockade of PD-1/PD-L1 axis may generate protective immunological memory in long-term survivors. A slight decrease in body weight was observed in the ^{68}Ga-DOTA-2P(FAPI)$_2$/^{177}Lu-DOTA-2P(FAPI)$_2$ and combination therapy groups, followed by recovery after 6 days (figure 3E). Further characterization of the TME of CT26-FAP tumor transplants was performed. IHC staining of tumor tissues on day 7 post-showed the lowest percentage of Ki-67 and CD31 positive cells in this group, indicating reduced cell proliferation and decreased new blood vessel formation in tumors. A significant increase in the number of CD8+ T cells in the TME and enhanced activity of GZMB suggests a heightened antitumor immune response (figure 3F).
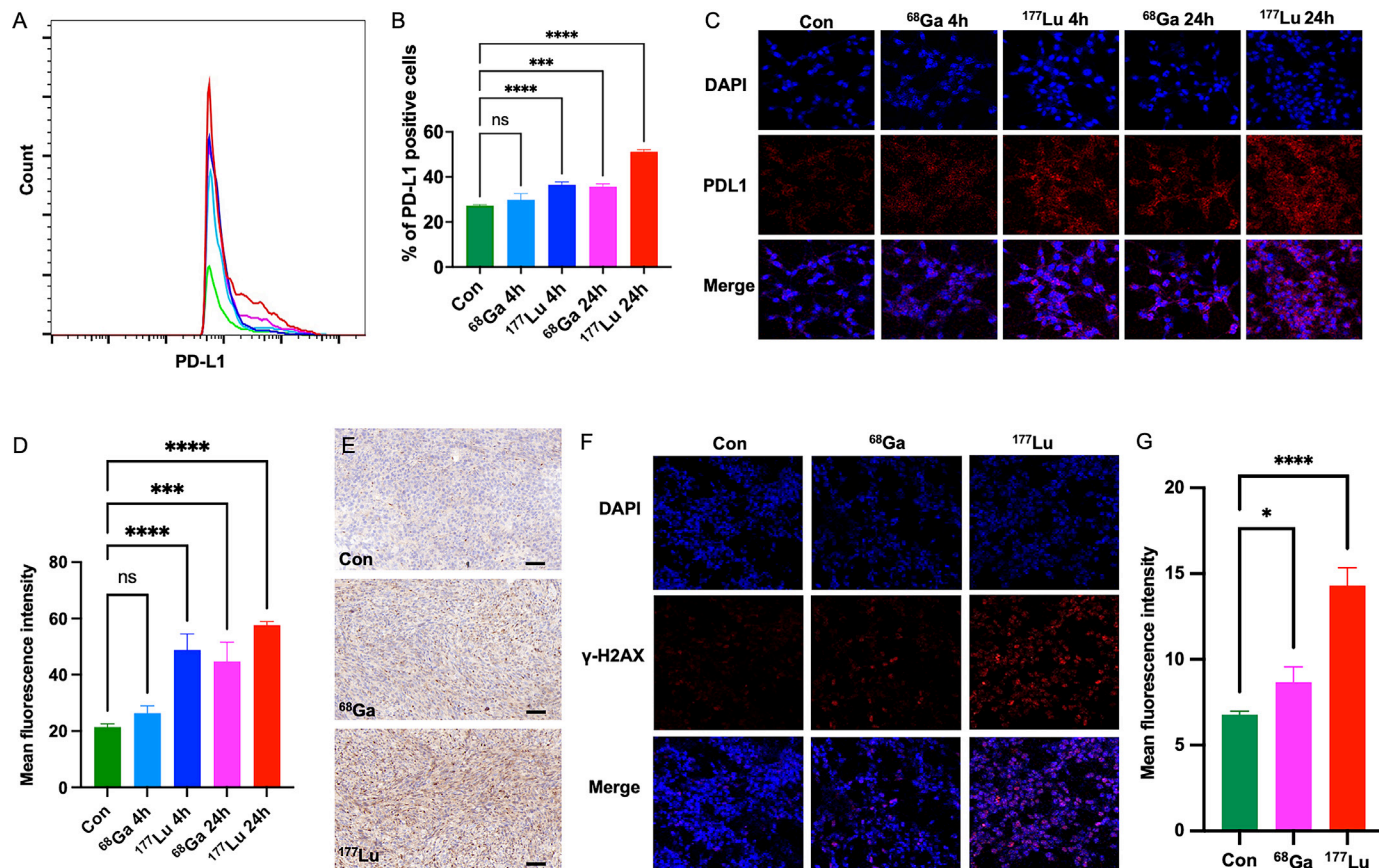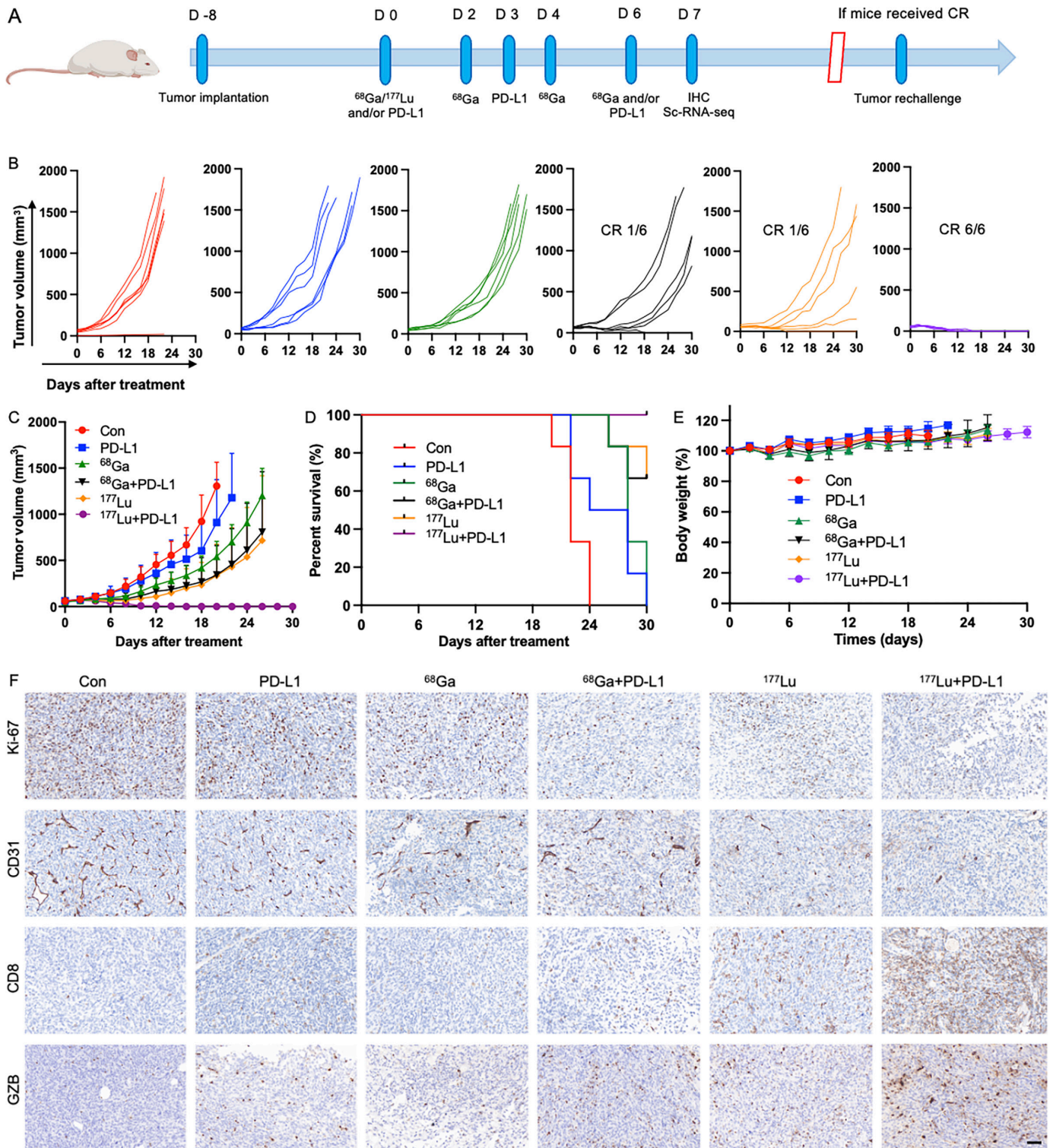
Figure 2 The ^{68}Ga/^{177}Lu-DOTA-2P(FAPI)$_2$ significantly upregulated PD-L1 both in vitro and in vivo. (A) Flow cytometry assessed and analyzed increased PD-L1 expression on CT26-FAP tumor cells after ^{68}Ga/^{177}Lu-DOTA-2P(FAPI)$_2$ stimulation at different time points. (B) Representative histograms were used to present the upregulation of PD-L1 after radiation stimulation (n=3/group). (C) Confocal images of PD-L1 immunofluorescence staining in CT26-FAP tumor cells at different time points after coincubation with ^{68}Ga/^{177}Lu/-DOTA-2P(FAPI)$_2$. (D) Representative histograms showed the upregulation of PD-L1 after radiation stimulation (n=3/group). (E) Immunohistochemical staining of PD-L1 in tumor tissues. Scale bar: 50 μm. (F) Confocal images of γ-H2AX immunofluorescence staining in CT26-FAP tumor cells after coincubation with ^{68}Ga/^{177}Lu/-DOTA-2P(FAPI)$_2$. (G) Representative histograms showed the upregulation of γ-H2AX after ^{68}Ga/^{177}Lu/-DOTA-2P(FAPI)$_2$ stimulation (n=3/group).

Intratumoral cell types and intercellular communication revealed by scRNA-seq

We isolated single cells from the tumor tissues of CT26-FAP tumor-bearing mice from different treatment groups into single cells and performed scRNA-seq. After quality control and removal of doublets (online supplemental figure S2A, figure 4A,B), the unsupervised clustering of 70,808 cells identified 15 distinct clusters (online supplemental figure S2B). These clusters were further divided into eight major cell types: cancer cells, T cells, NK cells, CAFs, monocytes/macrophages, dendritic cells, neutrophils, and mast cells (figure 4A). Compared with the control group, the proportion of T-cells and NK cells was significantly higher in both the ^{177}Lu-DOTA-2P(FAPI)$_2$ therapy and combination therapy groups with ^{68}Ga/^{177}Lu-DOTA-2P(FAPI)$_2$ and αPD-L1 mAb (figure 4C). This indicates that these treatments effectively recruit T and NK cells to the TME, thereby enhancing immune regulation within the tumor. Notably, mice treated with ^{177}Lu-DOTA-2P(FAPI)$_2$ in combination with immunotherapy showed a higher proportion of T and NK cells than those treated with ^{68}Ga-DOTA-2P(FAPI)$_2$. This suggests that while

high-dose ^{68}Ga labeled radiopharmaceuticals combined with immunotherapy enhance the immune response within the TME, combination therapy with ^{177}Lu labeled radiopharmaceuticals is more effective in modulating the TME. The highest treatment efficacy was observed in the group receiving ^{177}Lu-DOTA-2P(FAPI)$_2$ combined with αPD-L1 mAb, which also exhibited a significantly increased proportion of neutrophils within the tumors compared with other groups. This observation suggests a potentially unique role for neutrophils in enhancing the efficacy of this combined therapeutic approach.

We analyzed the activation of cell-signaling pathways in the different treatment groups to explore the potential core-signaling pathways activated during the treatment response (figure 4D). The FASLG and IL1 pathways were significantly activated in the ^{177}Lu-DOTA-2P(FAPI)$_2$ radioligand therapy and ^{177}Lu-DOTA-2P(FAPI)$_2$ combined immunotherapy groups. These pathways are typically associated with antitumor activity,[17 18] suggesting that ^{177}Lu-DOTA-2P(FAPI)$_2$ radioligand therapy and combination therapy with ^{177}Lu-DOTA-2P(FAPI)$_2$ and αPD-L1 mAb can enhance the antitumor response. Conversely,

Figure 3 ^{68}Ga/^{177}Lu-DOTA-2P(FAPI)$_2$ radioligand therapy significantly enhanced the antitumor effect after combined with αPD-L1 mAb. (A) Illustration of the therapeutic regimen and treatment timelines for CT26-FAP tumor-bearing mice (n=6/group). (B) Individual tumor growth trajectories of CT26-FAP tumor-bearing mice across diverse treatment groups (n=6/group). (C) Tumor growth. (D) Survival rate. (E) Body weight graphs of CT26-FAP tumor-bearing mice in different treatment groups (n=6/group). (F) Immunohistochemical (IHC) staining for Ki-67, CD31, CD8+T, and GZMB in tumor tissues 7 days post-treatment. Scale bar: 50 µm. CR, complete remission.

the expression of SPP1 was significantly decreased, which is related to the proliferation, migration, and invasion of malignant tumors. We also evaluated changes in ligand-receptor interactions to detect differences in signaling between immune and tumor cells in the different treatment groups (figure 4E). The Tgfb1–(Tgfbr1+Tgfbr2) interaction between NK and cancer cells in both ^{177}Lu-DOTA-2P(FAPI)$_2$ radioligand therapy and
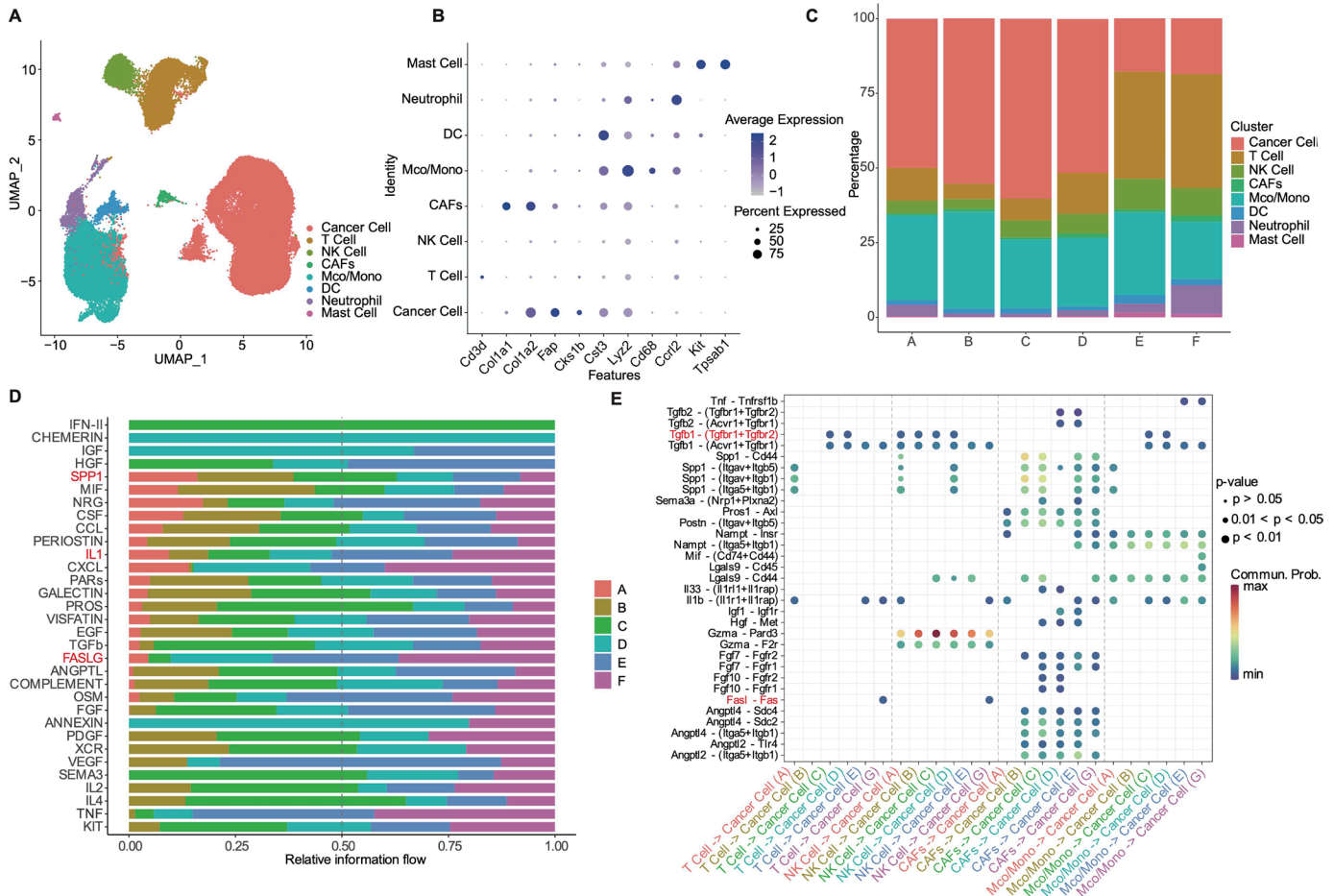
Figure 4 Cell type identification and different cell signaling pathways in the CT26-FAP tumor-bearing mice. (A) UMAP plot of all cells. (B) Dot plot reveals characteristic marker genes of different cell components. (C) Bar plot compares major cell lineages of different groups. (D) Bar plot depicts the proportions of different cell signaling pathways within different groups. (E) Highlighted ligand-receptor interactions between T-cells, NK cells, CAFs, Mco/Mono, and cancer cells.

^{177}Lu-DOTA-2P(FAPI)$_2$ combined with immunotherapy was silenced. This interaction is thought to promote tumor growth and metastasis by activating the TAK1/JNK/JUN-related pathway in tumor cells.[19] The Fasl-Fas interaction, involving T and NK cells with cancer cells, was active in the ^{177}Lu-DOTA-2P(FAPI)$_2$ combined immunotherapy group. This activation is associated with the induction of apoptosis in tumor cells.[20–22] It aligns with the optimal outcomes of combination therapy (figure 4E), consistent with the activation of the FASLG pathway shown in figure 4D.

Combining ^{177}Lu-DOTA-2P(FAPI)$_2$ with immunotherapy inhibits malignant progression and enhances immune function

We re-clustered tumor cells into four subgroups based on specific marker genes: high-cycle, low-cycle, invasive-, and complement-associated tumor cells (figure 5A, online supplemental figure S3A). Using RNA velocity calculations for cellular reprogramming, we identified a predominant evolutionary trajectory in which low-cycle tumor cells differentiated into high-cycle or invasive tumor cells, indicating a progressive trend toward malignancy (figure 5B). We conducted a detailed examination of the tumor cell subtypes within the three treatment groups

(D, E, and F): ^{68}Ga-DOTA-2P(FAPI)$_2$ in combination with αPD-L1 mAb, ^{177}Lu-DOTA-2P(FAPI)$_2$, and ^{177}Lu-DOTA-2P(FAPI)$_2$ in combination with αPD-L1 mAb that showed superior therapeutic outcomes, and the control group. Compared with group A, post-therapeutic observations indicated a reduction in low-cycle tumor cells and an increase in invasive tumor cells within groups D and E (figure 5C), suggesting that despite some degree of tumor growth suppression, the treatments may have inevitably promoted tumor malignancy and resistance. Conversely, group F maintained a stable count of low-cycle tumor cells and a consistent proportion of invasive tumor cells, indicating that the combined regimen of ^{177}Lu-DOTA-2P(FAPI)$_2$ and αPD-L1 mAb effectively inhibited the increase of various tumor cell subpopulations.

To evaluate the TME, we analyzed variations in tumor transcription factors across treatment groups using the SCENIC protocol. The heat map illustrates the genes with significantly different expression levels in group F compared with the other groups (figure 5D). Among the groups showing enhanced antitumor efficacy (groups D, E, and F), transcription factors that inhibit tumor growth were consistently upregulated, with group F exhibiting
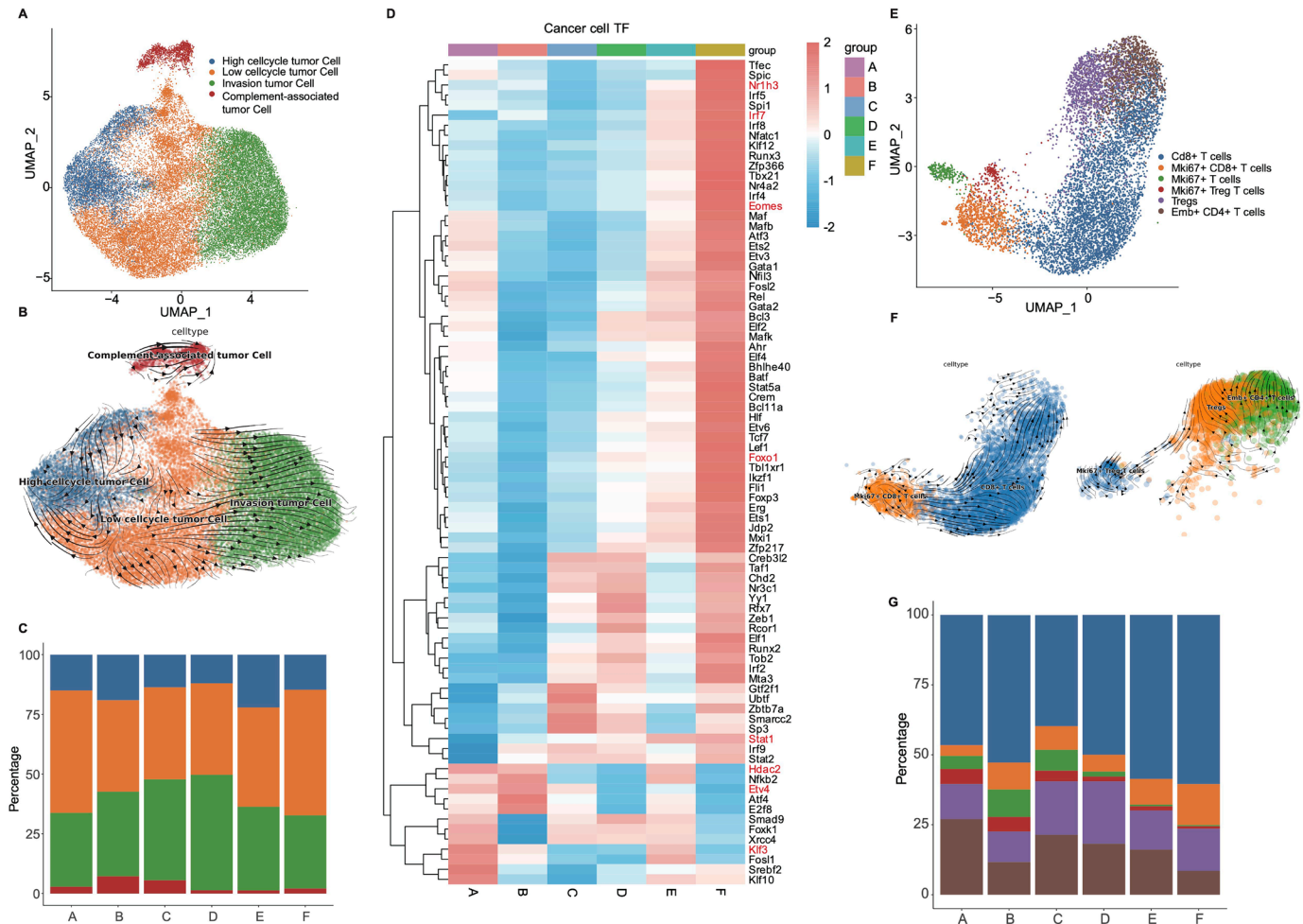
Figure 5 Cancer cell and T-cell characterization in CT26-FAP tumor-bearing mice. (A) UMAP plot of tumor cells. (B) RNA velocity analysis reflects the evolutionary process of tumor cells. (C) Bar plot illustrating the proportions of tumor cell subpopulations. (D) SCENIC analysis depicts the differential area under the curve values of transcription factors. (E) UMAP plot of T-cell subpopulations in CT26-FAP tumor-bearing mice. (F) RNA velocity analysis reflects the evolutionary process of T-cells. (G) Bar plot illustrating the proportions of T-cell subpopulations in each group.

the most significant increase. Critical factors such as Nr1h3, Irf7, Eomes, Foxo1, and Stat1 were significantly elevated in group F, consistent with previous research.[23–27] In contrast, factors implicated in tumor progression, namely Hdac2, Etv4, and Klf3, were significantly down-regulated.[28–30] These results highlight the potential of the combination treatment with ^{177}Lu-DOTA-2P(FAPI)$_2$ and αPD-L1 mAb to inhibit the malignant progression of cancer, suggesting a promising therapeutic pathway.

To further investigate the dynamics of immune cell subpopulations in different treatment groups, we analyzed six main subpopulations based on specific marker genes: CD8+ T cells, Mki67+ CD8+ T cells (proliferative effector T-cells), Mki67+ T cells, Mki67+ Treg T-cells (proliferative Tregs), Tregs, and Emb+ CD4+ T cells (figure 5E and online supplemental figure S2B).[31] RNA velocity analysis revealed the differentiation trajectories of CD8+ and CD4+ T cells, demonstrating their evolution from the proliferative to effector states (figure 5F). We conducted a detailed examination of T-cell subtypes within the three treatment groups (D, E, and F), demonstrating superior

therapeutic outcomes compared with the control group. Our findings revealed that the number of CD8+ T cells, in proliferative and effector forms, was significantly higher in groups D, E, and F than in the control group, with the most substantial increase observed in group F (figure 5G). To further investigate whether CD8+ T cells contribute to the synergistic killing of tumor cells in ^{177}Lu-DOTA-2P(FAPI)$_2$ treatment, we conducted a CD8+ T cell depletion experiment. The results showed that CD8+ T cell depletion significantly impaired the therapeutic efficacy of ^{177}Lu-DOTA-2P(FAPI)$_2$ when used as monotherapy (online supplemental figure S4). Regarding the total number of suppressive T-cells, including both Mki67+ Treg T-cells and Tregs, there was an increase in group D and a decrease in groups E and F. Notably, group F not only showed the highest activation of tumor-killing CD8+ T cells but also exhibited a reduced proportion of suppressive T-cells. This suggests that the treatment regimen in group D partially enhanced the antitumor immune response. In contrast, the treatment regimen in group F was most effective in promoting the activation of
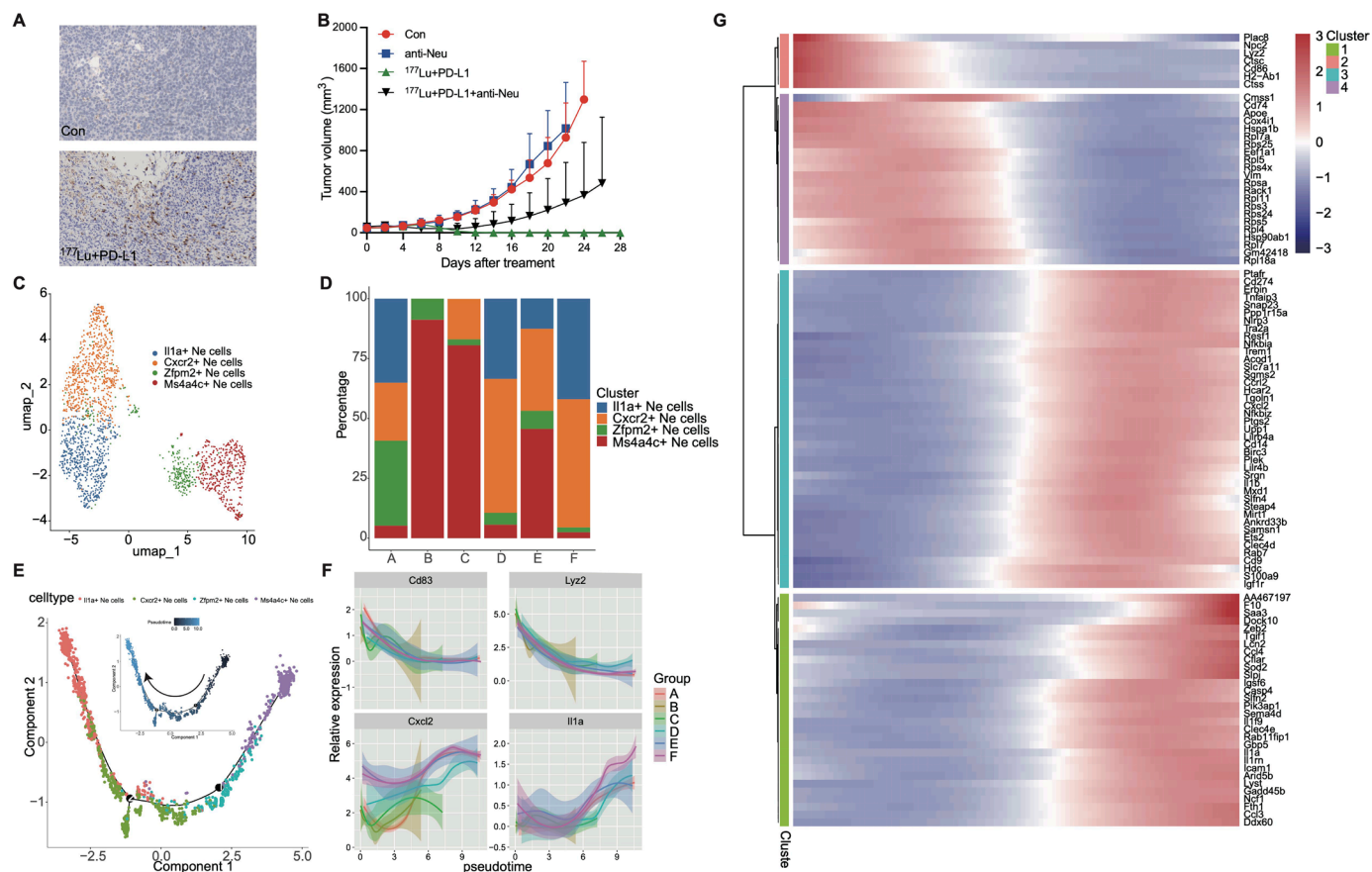
Figure 6 Intratumor mature neutrophils exert coordinated antitumor effects and their mechanisms. (A) Immunohistochemical staining of Ly6G in tumor samples. (B) Tumor growth curves of CT26-FAP tumor-bearing mice after blockade of neutrophil. (C) UMAP plots of neutrophil clusters. (D) Bar charts illustrating the distribution of neutrophil subpopulations. (E) Monocle2 pseudo-temporal analysis reveals the evolutionary trends within neutrophil subclusters. (F) Trajectory changes in expression levels of key genes at various cellular stages in neutrophils. (G) Heatmap of the top differentially expressed genes in neutrophils throughout pseudotime.

effector T-cells capable of targeting tumors. Additionally, it significantly reduced the suppressive effect of Tregs on immune responses.

Mature neutrophils subgroup enhanced the therapeutic efficacy against tumors

In our analysis of total cell subgroups (figure 4C), we observed a significant increase in the number of neutrophils in group F, which received a combination therapy of ^{177}Lu-DOTA-2P(FAPI)$_2$ and αPD-L1 mAb, compared with the control group. This increase was further confirmed by IHC (figure 6A). The in-vitro cytotoxicity of neutrophils subtype (N1 type) against tumor cells was confirmed by extracting and stimulating neutrophils from the bone marrow of BALB/c mice, following established protocols from the literature.[32] After co-culturing these N1 neutrophils with CT26-FAP cells, cytotoxic effects were assessed using both an ATP Luminescent Cell Viability Assay and a Calcein AM/PI Live-Dead Cell Staining Assay. The results supported our hypothesis, demonstrating a significant reduction in the viability of CT26-FAP cells and an increase in dead CT26-FAP cells in the co-culture, as shown in online supplemental figure S5. To assess the role of neutrophils in the efficacy of the combination

therapy, we implemented an anti-neutrophil blockade in-vivo. While the blockade alone did not affect tumor growth, its integration into combination therapy markedly diminished the antitumor response (figure 6B). This indicates that neutrophils are essential for mediating the antitumor effects of combination therapy.

Further investigation revealed four distinct neutrophil subpopulations within the tumor tissue: Il1a+, Cxcr2+, Zfpm2+, and Ms4a4c+ Ne cells (figure 6C, online supplemental figure S6A). Notably, Il1a+ Ne and Cxcr2+ Ne cells, markers of mature neutrophils known for their pro-inflammatory properties,[33 34] were most prevalent in group F (figure 6D). Our pseudo-time analysis (figure 6E) traced the developmental trajectory of these neutrophils from immature (Zfpm2+ and Ms4a4c+ Ne cells) to mature forms (Il1a+ and Cxcr2+ Ne cells). RNA velocity analysis corroborated these findings, identifying Ms4a4c+ Ne cells at the initial stage and Il1a+ Ne cells at the mature stage of development (online supplemental figure S6B). We observed that the early development markers Cd83 and Lyz2 were highly expressed initially and decreased over time (figure 6F).[35 36] In contrast, genes associated with antitumor effects, such as CXCL2

and IL1a, increased as the neutrophils matured, with the highest expression levels in group F. CXCL2 has been well demonstrated to recruit neutrophils under various physiological and pathological conditions.[37] Our results suggest that ^{177}Lu-DOTA-2P(FAPI)$_2$ combined with αPD-L1 mAb immunotherapy-induced CXCL2 expression is responsible for recruiting antitumor neutrophils to the TME.[38]

Gene expression dynamics analysis identified four major gene clusters consistent with pseudo-time progression (figure 6G). Early-stage neutrophils express developmental genes such as Lyz2. Multiple ribosomal proteins (RPs) related to protein synthesis were highly expressed in naïve neutrophils (figure 6G), indicating their development. As these cells mature, antitumor genes have notable upregulation, including il1a and icam1, which are critical for forming an inflammatory TME.[34 39] Our findings suggest that, in group F, neutrophils may directly kill tumor cells via the TNF family signaling pathway (online supplemental figure S6C). Additionally, neutrophils recruited more immune T cells through CCL4–CCR5 and CCL3–CCR5 receptor-ligand interactions (online supplemental figure S6C). These mechanisms have been corroborated in previous study.[40] These findings highlight the synergistic antitumor effects of mature neutrophil subpopulations in combination therapy.

DISCUSSION
Clinical trials have reported low response rates to ICIs alone, with only a minority of patients benefiting. We developed and tested a novel strategy to increase the sensitivity of FAP-expressing MSS-CRC to ICIs by modulating TME using FAP-targeting radiopharmaceuticals. Given that FAP is a pan-cancer target, these effects are presumed to be generalizable across a broad spectrum of tumor types. The combination of ^{177}Lu-DOTA-2P(FAPI)$_2$ radioligand therapy and αPD-L1 mAb immunotherapy demonstrated greater immune microenvironment modulation than the combination with ^{68}Ga-DOTA-2P(FAPI)$_2$. This significantly increased the rate of CR and prolonged overall survival. The combination therapy reprogrammed the TME and enhanced the immune response to PD-L1 inhibitor in a mouse model of MSS-CRC, enhancing antitumor intercellular communication and increasing the infiltration of CD8+ T cells and mature antitumor neutrophils while reducing regulatory T-cells and inhibiting the increase of various tumor cell subpopulations.

A previous study highlighted that the novel FAP-targeting dimeric molecule ^{177}Lu-DOTA-2P(FAPI)$_2$ exhibited increased tumor uptake, prolonged retention, and enhanced antitumor effects compared with the conventional FAPI monomeric molecule.[14 15] Moreover, in-vivo tumor uptake of radiopharmaceuticals may be influenced by differences in the data acquisition time-points and metal coordination between ^{177}Lu and ^{68}Ga, and not just the radionuclide's half-life (^{68}Ga $t_{1/2}$: 68 min, ^{177}Lu $t_{1/2}$: 6.7 days). In this study, radiation from both ^{68}Ga

and ^{177}Lu radiolabeled DOTA-2P(FAP)$_2$ induced DNA double-strand breaks and upregulated PD-L1 expression. We have previously explored the underlying mechanisms, with the activation of the NF-kB/IRF3 and STAT1/3-IRF1 pathways playing crucial roles in modulating PD-L1 expression following DNA damage and repair.[12] PD-L1 has been identified as a biomarker for the response to ICIs treatment and is routinely tested in clinical practice.[41] Thus, this combination is justified. Further, in vivo studies showed that ^{68}Ga/^{177}Lu-DOTA-2P(FAPI)$_2$ inhibited tumor growth and modulated the expression of PD-L1 in tumor tissues. As expected, the addition of PD-L1 immunotherapy further enhanced antitumor efficacy. Results also showed that the degree of DNA double-strand breaks, upregulation of PD-L1 expression, and antitumor efficacy of ^{177}Lu-DOTA-2P(FAPI)$_2$ were greater than those of ^{68}Ga-DOTA-2P(FAPI)$_2$. Moreover, the antitumor efficacy of PD-L1 combination therapy with ^{177}Lu-DOTA-2P(FAPI)$_2$ was greater than that with ^{68}Ga-DOTA-2P(FAPI)$_2$, significantly increasing the CR rate and prolonging overall survival. In our study, we increased the dose of ^{68}Ga-DOTA-2P(FAPI)$_2$ (29.6 MBq) to enhance its therapeutic effect as much as possible, given its limited capacity to kill tumor cells compared with ^{177}Lu. Even with the higher dose, our data clearly demonstrated that the antitumor efficacy and ability to reshape the immune microenvironment of ^{68}Ga were not as strong as those observed with ^{177}Lu-DOTA-2P(FAPI)$_2$ at 18.5 MBq. The superior efficacy of the ^{177}Lu-DOTA-2P(FAPI)$_2$ in combination therapy compared with the ^{68}Ga-DOTA-2P(FAPI)$_2$ can be attributed to several factors related to the physical and radiochemical properties of the isotopes, including longer half-life of ^{177}Lu, and greater tissue penetration range and greater upregulation of PD-L1 expression than those from the ^{68}Ga-treated group. Mice cured in these trials consistently exhibited tumor-specific memory. Preliminary results from the PD-L1 combination groups (combined with either ^{68}Ga-DOTA-2P(FAPI)$_2$ or ^{177}Lu-DOTA-2P(FAPI)$_2$) showed reduced tumor proliferation and angiogenesis and increased production of CD8+ T cells. This phenomenon was most pronounced in the combined treatment group with ^{177}Lu-DOTA-2P(FAPI)$_2$ and αPD-L1 mAb.

Consistent with the IHC results, scRNA-seq revealed a significant alteration in the tumor immune microenvironment in the "^{177}Lu-DOTA-2P(FAPI)$_2$+αPD-L1 mAb" combination therapy group, leading to an increase in the number of intratumorally infiltrating T cells, with the greatest increase observed in the proportion of effector T-cell subsets, which correlates with its optimal therapeutic efficacy and durable immune memory. Additionally, scRNA-seq indicated that the proportion of NK cells in TME increased following treatment in both "^{177}Lu-DOTA-2P(FAPI)$_2$" and "^{177}Lu-DOTA-2P(FAPI)$_2$+αPD-L1 mAb" groups, with significant upregulation of the antitumor-related FASLG pathway, while the tumor-promoting SPP1 pathway was significantly downregulated.[18] Moreover, several antitumor-related transcription factors, including

Nr1h3, Irf7, Eomes, Foxo1, and Stat1, were also found to be upregulated, indicating that this combination therapy significantly activated the antitumor response.[28–30] These data indicate that ^{177}Lu-DOTA-2P(FAPI)$_2$ in combination with αPD-L1 mAb is more effective in reversing the tumor immunosuppressive microenvironment and preventing the increase of various subpopulations of tumor cells.

Furthermore, our data showed that ^{177}Lu-DOTA-2P(FAPI)$_2$ in combination with αPD-L1 mAb significantly increased the proportion of neutrophils within the tumor. However, multiple neutrophil statuses with varying maturity, surface marker expression, and transcriptional profiles have been reported in cancers, making the antitumor and pro-tumor effects of neutrophils controversial.[42 43] However, some mature neutrophil subpopulations showed synergistic antitumor effects with previous studies. Our results show that the proportion of Il1a+ and Cxcr2+ mature neutrophil subpopulations associated with pro-inflammatory cytokines was higher in the combination therapy group than in the other groups. We hypothesized that neutrophils within the tumor were important effector cells exerting a coordinated antitumor response in the combination therapy of ^{177}Lu-DOTA-2P(FAPI)$_2$ with αPD-L1 mAb. After further depletion of neutrophils within the tumor, the results showed that the antitumor response to combination therapy was attenuated.

Another recent study reported that the combination therapy with αPD-L1 mAb and ^{177}Lu-FAP-2287 (FAP-targeting cyclic peptide) in an MCA205-FAP murine sarcoma model was able to enhance the responsiveness of ICIs by modulating the TME and increasing the recruitment of tumor-infiltrating CD8+ T cells.[44] This finding is consistent with our results of a significant increase in the number of tumor-infiltrating CD8+ T cells in the combination therapy group as analyzed by scRNA-seq. Therefore, we conclude that TRT is an immunomodulator that enhances tumor responsiveness to ICIs. We also compared the mechanisms of action of the diagnostic and therapeutic radionuclides. While ^{68}Ga-DOTA-2P(FAPI)$_2$ can induce DNA double-stranded breaks and apoptosis, its efficacy is less pronounced than that of ^{177}Lu-DOTA-2P(FAPI)$_2$. We conducted a deeper and more comprehensive analysis of the TME through scRNA-seq, which allowed us to identify cellular heterogeneity that may be masked at the population level. By analyzing the transcriptional activity of individual cells, we can reveal unknown subpopulations and unique cell states, facilitating our understanding of the trend of subgroup proportion in tumor cells, the degree of transcription factor enrichment, and the signaling pathways that may be activated from a genomic perspective. Importantly, mature neutrophils exerted synergistic antitumor effects in the combination therapy group.

It has been reported that 90% of naive lymphocytes can undergo apoptosis 2–8 hours after irradiation with a dose of 3 Gy EBRT, and these naive lymphocytes are more sensitive than most tumor cells.[45] Future studies should explore different combination approaches, such as the triple combination of TRT, ICI, and EBRT for primary or large tumor lesions and TRT and ICI for small metastatic tumors, to reduce off-target toxicity from EBRT. Ravi B. Patel and his team demonstrated that moderate-dose EBRT and low-dose TRT are complementary and non-redundant in enhancing the response of "cold" tumors to ICIs, especially in the presence of multiple metastatic tumors.[46] Moderate-dose EBRT mainly exerts its effects by initiating T-cell antigen recognition diversity through in situ vaccination. Furthermore, many preclinical studies have suggested that low-dose radiation is beneficial for actively modulating the immune microenvironment of tumors while reducing damage to radiation-sensitive immature immune cells and normal tissues in the body.[47 48] Given the significant difference in the immune effects of TRT and EBRT, and the fact that FAP is a widely present and highly expressed target in a variety of malignant tumors, we hypothesized that the combination of immunotherapy with low-dose FAP-targeted TRT and EBRT may be more effective in reversing the immune desertification phenomenon in "cold" tumors that expressing FAP.

However, this study had some limitations. First, the microenvironment of subcutaneous tumors may differ from that of spontaneous colon cancer. However, since our research includes immunotherapy, it is essential for us to use murine tumor cells in mice with fully intact immune systems. Due to the difficulties in establishing immune-competent mouse models with spontaneous FAP expression, similar studies have used transfected FAP-expressing murine tumor models, such as MCA205-mFAP and 4T1-FAP tumor cells.[44 49] Nevertheless, exploring spontaneous expression of FAP colon cancer models or in situ colon cancer models would provide clinically relevant information that warrants further study. Second, experiments using colon cancer models with multiple metastatic tumors may be more consistent with the research goal of combining TRT and ICIs therapies. Although this method cannot fully represent the immune microenvironment of tumors, it provides some reference value for studying FAP overexpression in MSS-CRC therapy. This study focused on the CT26 colon tumor model to be as close to the clinical reality as possible, which is low tumor mutational burden and responsive to ICIs alone, aligning with the poor results of immunotherapy alone in most patients with tumors in the clinical setting. As different cancer types have different levels of FAP expression, the dose and frequency of TRT administration must be balanced with the actual level of FAP expression in the tumor. Third, although the combination therapy group with ^{177}Lu-DOTA-2P(FAPI)$_2$ and αPD-L1 mAb demonstrated superior antitumor activity compared with the ^{177}Lu-DOTA-2P(FAPI)$_2$ alone, the tumor sizes at the time of treatment initiation were relatively small (approximately 50 mm³). However, tumor sizes of 40–100 mm³ are commonly used in the therapeutic

experiments.[12 50] Nevertheless, further experiments using larger tumors will be necessary to validate the efficacy of this combination therapy strategy.

Our results suggest that FAP-targeting radiopharmaceuticals, especially ^{177}Lu-DOTA-2P(FAP)$_2$, have the potential to significantly enhance the therapeutic efficacy and enables a translatable approach to promoting response to PD-1/PD-L1 inhibitors. This finding underscores the necessity for pilot clinical trials to comprehensively evaluate the effectiveness of combining ^{177}Lu-DOTA-2P(FAP)$_2$ with immunotherapy, potentially transforming the treatment landscape for challenging tumors.

Author affiliations
[1]Department of Nuclear Medicine and Minnan PET Center, Xiamen Cancer Center, The First Affiliated Hospital of Xiamen University, School of Medicine, Xiamen University, Xiamen, Fujian, China
[2]Department of Colorectal Tumor Surgery, Xiamen Cancer Center, The First Affiliated Hospital of Xiamen University, School of Medicine, Xiamen University, Xiamen, Fujian, China
[3]Department of Radiation Oncology, Xiamen Cancer Center, Xiamen Key Laboratory of Radiation Oncology, The First Affiliated Hospital of Xiamen University, School of Medicine, Xiamen University, Xiamen, Fujian, China
[4]Department of Oncology, The Second Affiliated Hospital of Jiaxing University, Jiaxing, Zhejiang, China
[5]Laboratory of Xiamen Cancer Hospital, The First Affiliated Hospital of Xiamen University, School of Medicine, Xiamen University, Xiamen, Fujian, China
[6]Departments of Diagnostic Radiology, Surgery, Chemical and Biomolecular Engineering, and Biomedical Engineering, Yong Loo Lin School of Medicine and College of Design and Engineering, National University of Singapore, Singapore
[7]Clinical Imaging Research Centre, Centre for Translational Medicine, Yong Loo Lin School of Medicine, National University of Singapore, Singapore
[8]Nanomedicine Translational Research Program, NUS Center for Nanomedicine, Yong Loo Lin School of Medicine, National University of Singapore, Singapore
[9]Institute of Molecular and Cell Biology, Agency for Science, Technology, and Research (A*STAR), Singapore

Contributors JC, YZ and YP are the co-first authors of this article. HC, LZ, XC and GS are co-corresponding authors of this article. HC is the guarantor.

Competing interests None declared.

Patient consent for publication Not applicable.

Ethics approval All animal care and experimental procedures were reviewed and approved by the Animal Care and Use Committee of the Xiamen University Laboratory Animal Center (Approval No. XMULAC20200140).

Provenance and peer review Not commissioned; externally peer reviewed.

Data availability statement No data are available.

ORCID iDs
Qicong Luo http://orcid.org/0000-0002-3282-5336
Xiaoyuan Chen http://orcid.org/0000-0002-9622-0870
Haojun Chen http://orcid.org/0000-0002-9101-8884

REFERENCES

1. Lan Y, Moustafa M, Knoll M, et al. Simultaneous targeting of TGF-β/PD-L1 synergizes with radiotherapy by reprogramming the tumor microenvironment to overcome immune evasion. *Cancer Cell* 2021;39:1388–403.
2. André T, Shiu K-K, Kim TW, et al. Pembrolizumab in Microsatellite-Instability-High Advanced Colorectal Cancer. *N Engl J Med* 2020;383:2207–18.
3. Nguyen M, Tipping Smith S, Lam M, et al. An update on the use of immunotherapy in patients with colorectal cancer. *Expert Rev Gastroenterol Hepatol* 2021;15:291–304.
4. Teng F, Kong L, Meng X, et al. Radiotherapy combined with immune checkpoint blockade immunotherapy: Achievements and challenges. *Cancer Lett* 2015;365:23–9.
5. Theelen W, Chen D, Verma V, et al. Pembrolizumab with or without radiotherapy for metastatic non-small-cell lung cancer: a pooled analysis of two randomised trials. *Lancet Respir Med* 2021;9:467–75.
6. Chen H, Zhao L, Fu K, et al. Integrin $\alpha_v\beta_3$-targeted radionuclide therapy combined with immune checkpoint blockade immunotherapy synergistically enhances anti-tumor efficacy. *Theranostics* 2019;9:7948–60.
7. Jaini S, Dadachova E. FDG for Therapy of Metabolically Active Tumors. *Semin Nucl Med* 2012;42:185–9.
8. Fang S, Wang J, Jiang H, et al. F]-labeled 2-deoxy-2-fluoro-d-glucose in a colon cancer mouse model. *Cancer Biother Radiopharm* 2010;25:733–40.
9. Moadel RM, Nguyen AV, Lin EY, et al. Positron emission tomography agent 2-deoxy-2-[18F]fluoro-D-glucose has a therapeutic potential in breast cancer. *Breast Cancer Res* 2003;5:R199–205.
10. Paul DM, Ghiuzeli CM, Rini J, et al. A pilot study treatment of malignant tumors using low-dose 18F-fluorodeoxyglucose (18F-FDG). *Am J Nucl Med Mol Imaging* 2020;10:334–41.
11. Bao Y, Zhai J, Chen H, et al. Targeting m[6]A reader YTHDF1 augments antitumour immunity and boosts anti-PD-1 efficacy in colorectal cancer. *Gut* 2023;72:1497–509.
12. Wen X, Shi C, Zeng X, et al. A Paradigm of Cancer Immunotherapy Based on 2-[18F]FDG and Anti–PD-L1 mAb Combination to Enhance the Antitumor Effect. *Clin Cancer Res* 2022;28:2923–37.
13. Zboralski D, Hoehne A, Bredenbeck A, et al. Preclinical evaluation of FAP-2286 for fibroblast activation protein targeted radionuclide imaging and therapy. *Eur J Nucl Med Mol Imaging* 2022;49:3651–67.
14. Zhao L, Niu B, Fang J, et al. Synthesis, Preclinical Evaluation, and a Pilot Clinical PET Imaging Study of ^{68}Ga-Labeled FAPI Dimer. *J Nucl Med* 2022;63:862–8.
15. Zhao L, Chen J, Pang Y, et al. Development of Fibroblast Activation Protein Inhibitor-Based Dimeric Radiotracers with Improved Tumor Retention and Antitumor Efficacy. *Mol Pharm* 2022;19:3640–51.
16. Zhou M, Xiang S, Zhao Y, et al. [^{68}Ga]Ga-AUNP-12 PET imaging to assess the PD-L1 status in preclinical and first-in-human study. *Eur J Nucl Med Mol Imaging* 2024;51:369–79.
17. Zhivaki D, Kagan JC. NLRP3 inflammasomes that induce antitumor immunity. *Trends Immunol* 2021;42:575–89.
18. Han C, Godfrey V, Liu Z, et al. The AIM2 and NLRP3 inflammasomes trigger IL-1-mediated antitumor effects during radiation. *Sci Immunol* 2021;6:eabc6998.
19. Zhang G, Gao Z, Guo X, et al. CAP2 promotes gastric cancer metastasis by mediating the interaction between tumor cells and tumor-associated macrophages. *J Clin Invest* 2023;133.

20 French LE, Tschopp J. Protein-based therapeutic approaches targeting death receptors. *Cell Death Differ* 2003;10:117–23.
21 Smyth MJ, Hayakawa Y, Takeda K, *et al*. New aspects of natural-killer-cell surveillance and therapy of cancer. *Nat Rev Cancer* 2002;2:850–61.
22 Blaes J, Thomé CM, Pfenning P-N, *et al*. Inhibition of CD95/CD95L (FAS/FASLG) Signaling with APG101 Prevents Invasion and Enhances Radiation Therapy for Glioblastoma. *Mol Cancer Res* 2018;16:767–76.
23 Endo-Umeda K, Nakashima H, Uno S, *et al*. Liver X receptors regulate natural killer T cell population and antitumor activity in the liver of mice. *Sci Rep* 2021;11:22595.
24 Roulois D, Loo Yau H, Singhania R, *et al*. DNA-Demethylating Agents Target Colorectal Cancer Cells by Inducing Viral Mimicry by Endogenous Transcripts. *Cell* 2015;162:961–73.
25 Emerson DA, Rolig AS, Redmond WL. Enhancing the Generation of Eomeshi CD8+ T Cells Augments the Efficacy of OX40- and CTLA-4–Targeted Immunotherapy. *Cancer Immunol Res* 2021;9:430–40.
26 Jiang J, Huang Z, Chen X, *et al*. Trifluoperazine Activates FOXO1-Related Signals to Inhibit Tumor Growth in Hepatocellular Carcinoma. *DNA Cell Biol* 2017;36:813–21.
27 Raja R, Wu C, Bassoy EY, *et al*. PP4 inhibition sensitizes ovarian cancer to NK cell-mediated cytotoxicity via STAT1 activation and inflammatory signaling. *J Immunother Cancer* 2022;10:e005026.
28 Krauß L, Urban BC, Hastreiter S, *et al*. HDAC2 Facilitates Pancreatic Cancer Metastasis. *Cancer Res* 2022;82:695–707.
29 Zhu J, Teng H, Zhu X, *et al*. Pan-cancer analysis of Krüppel-like factor 3 and its carcinogenesis in pancreatic cancer. *Front Immunol* 2023;14:1167018.
30 Xie M, Lin Z, Ji X, *et al*. FGF19/FGFR4-mediated elevation of ETV4 facilitates hepatocellular carcinoma metastasis by upregulating PD-L1 and CCL2. *J Hepatol* 2023;79:109–25.
31 Yang H, Iwanaga N, Katz AR, *et al*. Embigin Is Highly Expressed on CD4+ and CD8+ T Cells but Is Dispensable for Several T Cell Effector Responses. *Immunohorizons* 2024;8:242–53.
32 Ohms M, Möller S, Laskay T. An Attempt to Polarize Human Neutrophils Toward N1 and N2 Phenotypes *in vitro Front Immunol* 2020;11:532.
33 Bajrami B, Zhu H, Kwak H-J, *et al*. G-CSF maintains controlled neutrophil mobilization during acute inflammation by negatively regulating CXCR2 signaling. *J Exp Med* 2016;213:1999–2018.
34 Malik A, Kanneganti T-D. Function and regulation of IL-1α in inflammatory diseases and cancer. *Immunol Rev* 2018;281:124–37.
35 Salcher S, Sturm G, Horvath L, *et al*. High-resolution single-cell atlas reveals diversity and plasticity of tissue-resident neutrophils in non-small cell lung cancer. *Cancer Biology* [Preprint] 2022.
36 Malengier-Devlies B, Metzemaekers M, Wouters C, *et al*. Neutrophil Homeostasis and Emergency Granulopoiesis: The Example of Systemic Juvenile Idiopathic Arthritis. *Front Immunol* 2021;12:766620.
37 Metzemaekers M, Gouwy M, Proost P. Neutrophil chemoattractant receptors in health and disease: double-edged swords. *Cell Mol Immunol* 2020;17:433–50.
38 Chan Y-T, Tan H-Y, Lu Y, *et al*. Pancreatic melatonin enhances anti-tumor immunity in pancreatic adenocarcinoma through regulating tumor-associated neutrophils infiltration and NETosis. *Acta Pharm Sin B* 2023;13:1554–67.
39 Vadillo E, Mantilla A, Aguilar-Flores C, *et al*. The invasive margin of early-stage human colon tumors is infiltrated with neutrophils of an antitumoral phenotype. *J Leukoc Biol* 2023;114:672–83.
40 Luther SA, Cyster JG. Chemokines as regulators of T cell differentiation. *Nat Immunol* 2001;2:102–7.
41 Mok TSK, Wu Y-L, Kudaba I, *et al*. Pembrolizumab versus chemotherapy for previously untreated, PD-L1-expressing, locally advanced or metastatic non-small-cell lung cancer (KEYNOTE-042): a randomised, open-label, controlled, phase 3 trial. *Lancet* 2019;393:1819–30.
42 Ng MSF, Kwok I, Tan L, *et al*. Deterministic reprogramming of neutrophils within tumors. *Science* 2024;383:eadf6493.
43 Takeshima T, Pop LM, Laine A, *et al*. Key role for neutrophils in radiation-induced antitumor immune responses: Potentiation with G-CSF. *Proc Natl Acad Sci USA* 2016;113:11300–5.
44 Zboralski D, Osterkamp F, Christensen E, *et al*. Fibroblast activation protein targeted radiotherapy induces an immunogenic tumor microenvironment and enhances the efficacy of PD-1 immune checkpoint inhibition. *Eur J Nucl Med Mol Imaging* 2023;50:2621–35.
45 Nakamura N, Kusunoki Y, Akiyama M. Radiosensitivity of CD4 or CD8 positive human T-lymphocytes by an in vitro colony formation assay. *Radiat Res* 1990;123:224–7.
46 Patel RB, Hernandez R, Carlson P, *et al*. Low-dose targeted radionuclide therapy renders immunologically cold tumors responsive to immune checkpoint blockade. *Sci Transl Med* 2021;13:eabb3631.
47 Liu S-Z. Nonlinear dose-response relationship in the immune system following exposure to ionizing radiation: mechanisms and implications. *Nonlinearity Biol Toxicol Med* 2003;1:71–92.
48 Rodriguez-Ruiz ME, Garasa S, Rodriguez I, *et al*. Intercellular Adhesion Molecule-1 and Vascular Cell Adhesion Molecule Are Induced by Ionizing Radiation on Lymphatic Endothelium. *Int J Radiat Oncol Biol Phys* 2017;97:389–400.
49 Fu Q, Gu Z, Shen S, *et al*. Radiotherapy activates picolinium prodrugs in tumours. *Nat Chem* 2024;16:1348–56.
50 Wang J, Sanmamed MF, Datar I, *et al*. Fibrinogen-like Protein 1 Is a Major Immune Inhibitory Ligand of LAG-3. *Cell* 2019;176:334–47.